Dynamic domain wall chirality rectification by rotating magnetic fields

Andre Bisig,[1,2,3,4,5,6,a)] Mohamad-Assaad Mawass,[2,5] Martin Stärk,[1,3,4] Christoforos Moutafis,[1,3,4] Jan Rhensius,[1,3] Jakoba Heidler,[1,3,4] Sebastian Gliga,[3,7] Markus Weigand,[2] Tolek Tyliszczak,[8] Bartel Van Waeyenberge,[9] Hermann Stoll,[2] Gisela Schütz,[2] and Mathias Kläui[1,3,4,5,b)]

[1]*Department of Physics, University of Konstanz, 78457 Konstanz, Germany*
[2]*Max Planck Institute for Intelligent Systems, 70569 Stuttgart, Germany*
[3]*Paul Scherrer Institute, 5232 Villigen PSI, Switzerland*
[4]*Institute of Condensed Matter Physics, École Polytechnique Fédérale de Lausanne, 1015 Lausanne, Switzerland*
[5]*Institute of Physics, Johannes Gutenberg University of Mainz, 55099 Mainz, Germany*
[6]*IBM Research - Zurich, 8803 Rüschlikon, Switzerland*
[7]*Laboratory for Mesoscopic Systems, Department of Materials, ETH Zurich, 8093 Zurich, Switzerland*
[8]*Advanced Light Source, LBNL, Berkeley, California 94720, USA*
[9]*Department of Solid State Sciences, Ghent University, 9000 Ghent, Belgium*

(Received 3 November 2014; accepted 3 March 2015; published online 23 March 2015)

We report on the observation of magnetic vortex domain wall chirality reversal in ferromagnetic rings that is controlled by the sense of rotation of a magnetic field. We use time-resolved X-ray microscopy to dynamically image the chirality-switching process and perform micromagnetic simulations to deduce the switching details from time-resolved snapshots. We find experimentally that the switching occurs within less than 4 ns and is observed in all samples with ring widths ranging from 0.5 μm to 2 μm, ring diameters between 2 μm and 5 μm, and a thickness of 30 nm, where a vortex domain wall is present in the magnetic onion state of the ring. From the magnetic contrast in the time-resolved images, we can identify effects of thermal activation, which plays a role for the switching process. Moreover, we find that the process is highly reproducible so that the domain wall chirality can be set with high fidelity. © *2015 AIP Publishing LLC*. [http://dx.doi.org/10.1063/1.4915256]

The controlled manipulation of magnetic domain walls in nanowires has potential for data storage[1] and domain wall logic.[2,3] For example, in the proposed racetrack memory and logic devices, one data bit is represented by the presence or absence of a magnetic domain wall.[1] To implement domain wall logic operations, the position of the domain walls is controlled by spin-polarized currents injected through straight nanowires[1,3,4] or by rotating magnetic fields and domain walls traveling through a complex network of curved nanowires.[2] In magnetic nanowires, there are typically two basic types of domain walls:[5,6] the *transverse domain wall*, where the magnetization continuously rotates in-plane, and the *vortex domain wall*, where the magnetization curls in-plane around the central vortex core. The magnetization within the vortex core points perpendicularly to the plane to reduce exchange energy,[7] and is either parallel ($p = +1$) or anti-parallel ($p = -1$) to the z-direction, defining the vortex core polarity p. The sense of rotation of the in-plane magnetization component, either counter-clockwise (CCW) or clockwise (CW), defines the vortex chirality $c = +1$ or $c = -1$, respectively. Therefore, using vortex domain walls, two data bits can be represented by the vortex core polarity $p = \pm 1$ and the vortex chirality $c = \pm 1$.[8,9] The chirality can be used to define the path (or trajectory) of domain walls traveling in magnetic branched networks[10] and to control the domain wall position, the use of artificial pinning sites, such as notches or stray fields from neighbouring elements, has been suggested.[6] However, the dynamic pinning at such sites strongly depends on the detailed domain wall structure, in particular, the chirality of the vortex domain walls.[11–14] To reliably operate devices based on the motion of vortex domain walls, the domain wall chirality must thus be controllable. It can be set by using the ends of magnetic nanowires as chirality rectifiers.[15] However, for this to work, the vortex domain walls must be trapped at an impasse. Alternatively, the chirality of nucleated vortex domain walls can be controlled by the direction of a saturating field in an optimized injection pad,[16] or by the combination of a well tuned spatially confined field generated by an injection line and a notch in the magnetic nanowire.[10] But these methods are cumbersome for real device applications, where the chirality needs to be set during the motion of the wall, and thus, a different approach is needed.

In this letter, we report experimental observation that the vortex domain wall chirality is fundamentally controlled by the sense of rotation of a rotating magnetic field in circular nanowires. Using time-resolved scanning transmission X-ray microscopy (STXM), we dynamically image vortex domain walls driven by rotating magnetic fields and find that the domain wall chirality switches after a reversal of the sense of rotation of the field. By comparing the time-resolved images with micromagnetic simulations, we find that the dynamic chirality-switching process is triggered by the nucleation of a vortex-antivortex core pair and is thermally activated. The observed switching is a result of the interplay between a dynamic distortion of the vortex domain wall structure and the radial magnetic field.

The permalloy ($Ni_{80}Fe_{20}$) rings, in which we study the domain wall motion and structure transformations, are 500–750 nm wide, 30 nm thick, and were fabricated on top of a 100 nm thick X-ray transparent Si_3N_4 membrane by

a)andre.bisig@gmail.com
b)klaeui@uni-mainz.de

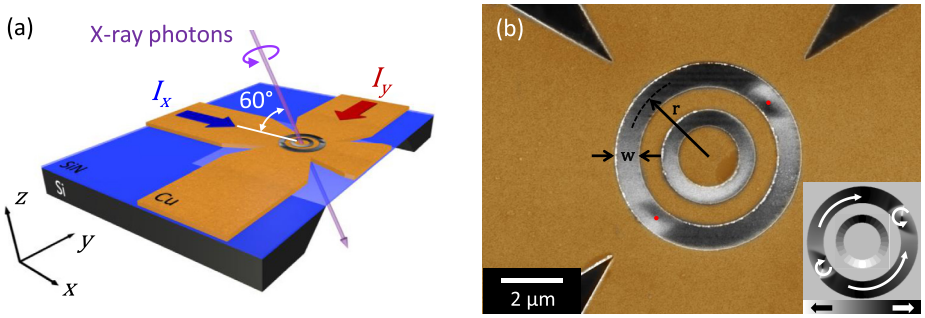

FIG. 1. (a) Schematic of the experimental setup. The in-plane magnetic field is generated by the currents $I_{x,y}$ in the crossed stripline. (b) Scanning electron micrograph (SEM) of the sample under investigation. The crossed-stripline is copper colored. The permalloy rings are fabricated below the copper striplines. A scanning transmission X-ray microscopy image showing the magnetic configuration is overlaid with the SEM image. Black (white) contrast corresponds to magnetization pointing to the right (left). The positions of the vortex cores are indicated by the red dots.

e-beam lithography, molecular beam evaporation in UHV, and lift-off processing, see Fig. 1(b). A 2 nm thick Au capping layer is used to prevent oxidation of the permalloy. For the generation of in-plane magnetic fields, 150 nm thick copper crossed-striplines were patterned on top of the rings, see Fig. 1. The ring dimensions (width and thickness) are chosen such that after saturation with a uniform external magnetic field, two vortex domain walls are formed.[6,17,18] The ferromagnetic ring is then in the so-called *onion state*.[17] When an in-plane external magnetic field **B** is applied, the Zeeman energy is minimal when the two domain walls align with the applied field. The energy depends on the angle θ between the field and the azimuthal position of the two vortex domain walls.[19] By rotating the applied field, the positions of the two energy minima propagate, leading to a circular motion of the domain walls along the ring and providing a way to control their positions.[19]

To generate an in-plane rotating magnetic field $\mathbf{B}(t) = B \cdot(\sin(2\pi ft), \cos(2\pi ft), 0)$ with frequency f and field strength B, two sinusoidal currents with 90° phase shift are injected through the crossed-stripline, as illustrated in Fig. 1(a). To isolate the currents flowing horizontally and vertically and to ensure equal current densities, we use an 180° power splitter to antisymmetrically inject the currents and maintain virtual ground at the center of the crossed-stripline. Because of inhomogeneous currents inside the stripline, the magnetic field is not constant, but can have an effectively elliptically varying amplitude away from the center of the stripline. Using finite-element calculations, we can estimate the difference of the in-plane components of the magnetic field to be less than 10% across the area occupied by the nanorings.[20]

In a first step, we imaged vortex domain walls in 500 nm wide rings with radii $r = 3\ \mu$m and $r = 5\ \mu$m after the injection of a CW and a CCW rotating magnetic field burst pulse with a rotation frequency of 12 MHz and an amplitude of $B = 6.1$ mT, see Fig. 2. The domain walls were imaged with sub-30-nm spatial resolution using STXM at the Advanced Light Source in Berkeley, CA, USA (beamline 11.0.2)[21] and at the MAXYMUS endstation, Helmholtz Zentrum Berlin, BESSY II, Germany. The in-plane magnetization component was imaged by tilting the sample surface normal by 30° with respect to the photon propagation direction and with contrast due to the X-ray magnetic circular dichroism (XMCD) effect.[22] The data were recorded at the Ni L3-absorption edge (852.7 eV). We see that after switching the sense of rotation of the magnetic field burst pulse from CW to CCW, the chirality of all vortex domain walls has reversed (cf. Figs. 2(a) and 2(b)). For instance, the head-to-head vortex domain wall at position (1) has a positive chirality ($c = +1$) after a full rotation in CW direction. During a subsequent injection of a CCW rotating magnetic field burst pulse, the domain wall travels around the ring in CCW direction to position (4) and after the pulse, its chirality has switched to $c = -1$. The opposite is the case for the tail-to-tail vortex domain wall at position (2). It has negative chirality ($c = -1$) after a CW rotation and positive chirality ($c = +1$) after a CCW rotation at position (3). Note that in a symmetric onion state, the two

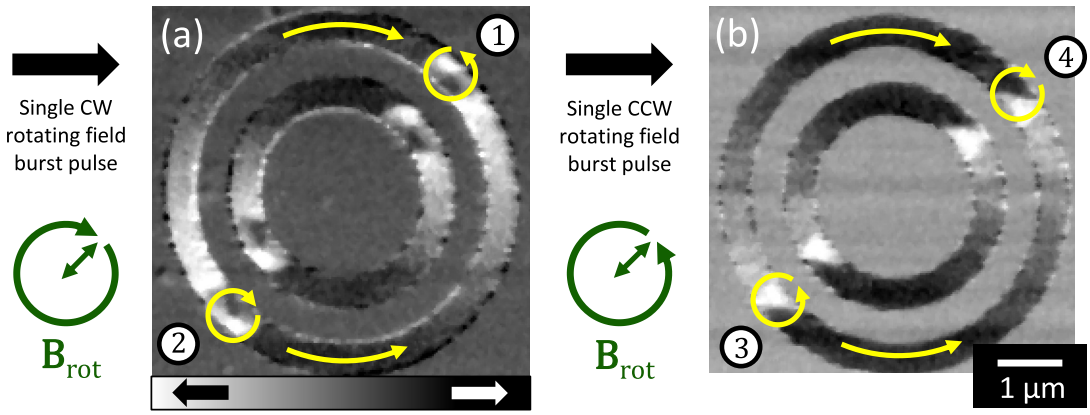

FIG. 2. STXM-XMCD images of four vortex domain walls in two nanorings (a) after the injection of a CW-rotating magnetic field burst pulse and (b) after a subsequent injection of a CCW-rotating magnetic field burst pulse. Black (white) contrast corresponds to magnetization pointing to the right (left). The yellow arrows indicate the direction of the magnetization.

diametrically opposed vortex domain walls always have opposite chiralities.

To investigate this switching mechanism in detail, we dynamically imaged the propagation of vortex domain walls driven by rotating magnetic field burst pulses with alternating sense of rotation. The studied nanoring is 750 nm wide with a radius of $r = 2.25\ \mu$m, see Fig. 1(b). The smaller inner ring is in the vortex state that has zero stray fields, and is thus disregarded for the following discussion. The dynamic domain wall propagation was imaged in a stroboscopic scheme, in which a snapshot of the moving domain walls is taken every 2 ns.[23] The temporal resolution of a single frame is limited by the electronics jitter ≈250 ps. The repetition rate of the stroboscopic experiment was 425 kHz, and the transmission signal was recorded over more than 10^9 consecutive pulse cycles. The rotation frequency of the magnetic field burst pulses is $f = 5$ MHz and the amplitude is $B = 6.8$ mT. The results are shown in Fig. 3(b) and the complete series of time-resolved images can be found as supplementary movie S1.[24] First, between $t = 0$ ns and 50 ns, the equilibrium position of the vortex core moves towards the outer edge of the ring as the external field ramps up from 0 mT to 6.8 mT along a 45° angle, as illustrated in Fig. 3(c). Next, the field starts to rotate CCW, and during the next 10 ns the vortex core gyrates CW around the moving quasi-static equilibrium position. The sense of gyration, either CCW or CW, is determined by the vortex core polarity $p = +1$ or $p = -1$, respectively.[25,26] The chirality-switching process starts at $t = 62$ ns and is finished at $t = 66$ ns, as indicated by the snapshots framed in red in Fig. 3(b). Note that during this switching process, the image contrast at the leading and the trailing edge of the vortex domain wall is slightly blurred. As with all switching mechanisms, the exact time and evolution depend on thermal activation,[12,27] which shifts the reversal in time and modifies the evolution leading to additional blurring of the image that is averaged across all repetitions. Following the switching process ($t = 116$ ns), the vortex domain wall chirality is reversed, and the domain wall propagates above the Walker breakdown in a precessional motion[23] until the field-rotation stops at $t = 250$ ns. Finally, the field ramps down from 6.8 mT to 0 ns during $t = 250$ ns to 300 ns. Then, this process repeats with the opposite and alternating sense of rotation of the rotating field pulse.

To reveal the switching process, we performed micromagnetic simulations using the object oriented micromagnetic framework (OOMMF).[28] Often such micromagnetic simulations of curved geometries lead to artifacts due to the cubic discretization of a curved surface that can entail artificial pinning. Thus, the critical issue is to reduce the pinning due to cell discretization of the leading and trailing half-antivortices of the vortex domain wall that travel along the nanoring edges. For this, we define a smooth profile of the saturation magnetization $M_S(\mathbf{r})$ at position $\mathbf{r} = (x, y)$ along the cross-section of the nanowire

$$M_S(\mathbf{r}) = \frac{M_S}{2}\left[\tanh\left(\frac{x^2 + y^2 - r_i^2}{d^2}\right) + \tanh\left(\frac{-x^2 - y^2 + r_a^2}{d^2}\right)\right], \tag{1}$$

where $r_i = 1.875\ \mu$m and $r_a = 2.625\ \mu$m are the inner and outer radii of the nanoring, respectively, and $d^2 = 8\ \text{nm}^2$. The dimensions of the simulated ring are the same as in the experiment (width 750 nm and thickness 30 nm) and the cell

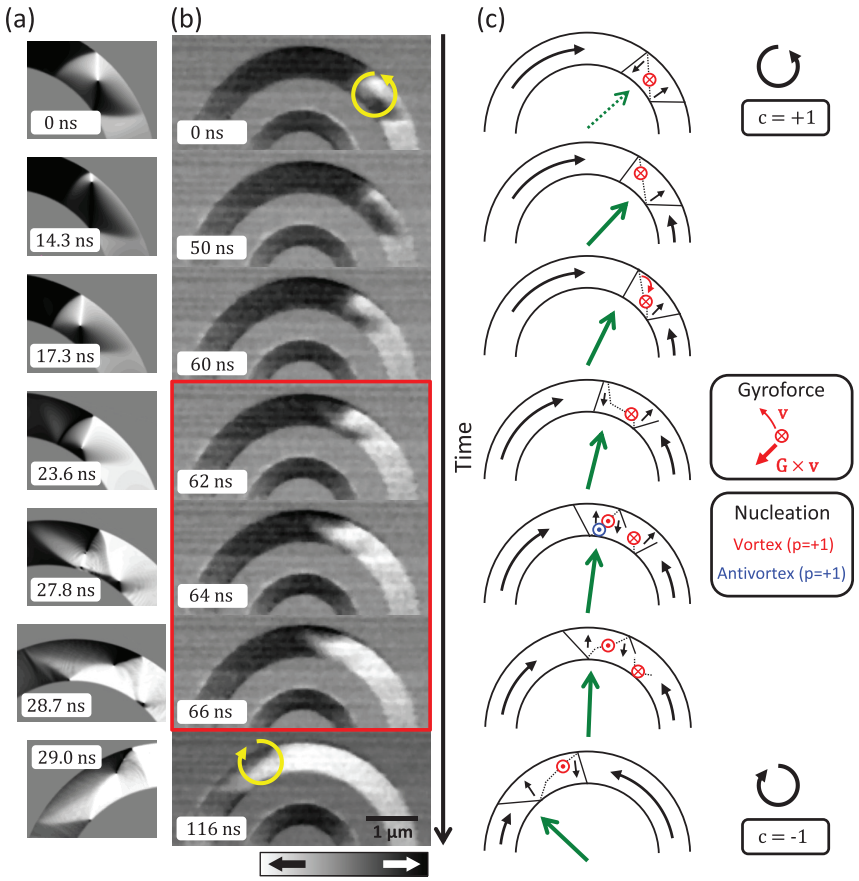

FIG. 3. Dynamic vortex domain wall chirality-switching process. (a) Micromagnetic simulations ($t = 0$–29.0 ns) of a vortex domain wall driven by a rotating magnetic field pulse ($f = 18$ MHz and $B = 14$ mT). (b) Time-resolved STXM images ($t = 0$ ns–116 ns) during the application of a rotating magnetic field pulse ($f = 5$ MHz and $B = 6.8$ mT). Black (white) contrast corresponds to magnetization pointing to the right (left). The chirality-switching process is highlighted by the snapshots with red frames (62 ns–66 ns). (c) Schematic representation of the chirality-switching process.

size is $5 \times 5 \times 30\,\text{nm}^3$. The material parameters used are typical for permalloy:[29] $M_S = 800 \times 10^3$ A/m, exchange stiffness $A = 1.3 \times 10^{-11}$ J/m, damping parameter $\alpha = 0.008$, no uniaxial anisotropy. When using the experimental field-rotation frequency and amplitude ($f = 5$ MHz and $B = 6.8$ mT), we could not reproduce the switching of the vortex domain wall chirality. And for rotation frequencies above 14 MHz, the switching processes can involve the nucleation and annihilation of multiple vortex-antivortex core pairs[30,31] or switching of the vortex core polarity, when the vortex core velocity exceeds ≈300 m/s.[32,33] By choosing a rotation frequency of 18 MHz and a field strength of 14 mT, the chirality-switching mechanism as observed experimentally can be reproduced.

In the following discussion, we refer to the vortex domain wall structure in the 2D model,[34] where the vortex domain wall can be understood as a composite quasi-particle with a central vortex core that is surrounded by the leading and trailing transverse domain walls, each consisting of a half-antivortex at the inner or outer etch of the nanoring, respectively, and a 90°-Néel wall domain wall boundary. Snapshots of the micromagnetic simulation are shown in Fig. 3(a), and a complete movie of the simulation can be found as supplementary movie S2.[24] We now compare these snapshots from the micromagnetic simulations (Fig. 3(a)) with the time-resolved images from the experiment (Fig. 3(b)) to deduce the chirality-switching process that is illustrated in Fig. 3(c). The reversal process starts at $t = 23.6$ ns (corresponding to $t = 62$ ns in the experiment, see Fig. 3(b)), the initial configuration is fixed ($p = -1$ and $c = +1$), because the vortex domain wall is in the stable configuration after clockwise rotation of the driving field, where the vortex chirality and vortex core polarity do not alternate.[23] The chirality reversal mechanism is governed by the dynamics of the vortex core and the vortex core motion is described by the Thiele model for steady-state motion of magnetic domains.[25,26] The vortex core intrinsically has a non-zero gyrovector $\mathbf{G} = -pG\hat{\mathbf{e}}_z$, pointing anti-parallel to the vortex core polarity, which is principally important for vortex dynamics description.[35,36] Following the Thiele model, a gyroforce $\mathbf{G} \times \mathbf{v}$ perpendicular to the vortex core velocity $\mathbf{v}$ and in the plane of the nanowire acts on the moving vortex core. Because the vortex core polarity is initially $p = -1$ and the velocity is tangentially along the ring, the gyroforce points towards the center of the nanoring, as schematically shown in Fig. 3(c). On the other hand, the parabolic restoring potential from the shape anisotropy[23] pushes the vortex core towards the center of the nanoring and acts against gyroforce. At $t = 27.8$ ns (64 ns), a vortex core ($p = +1$) and an antivortex core ($p = +1$) nucleate within the leading 90°-Néel wall, as shown, in detail, in Fig. 4. Because the gyroforces of a vortex core and an antivortex core point in opposite directions, the vortex core and antivortex core separate. At $t = 28.7$ ns (66 ns), the original vortex core ($p = -1$) annihilates with the trailing half-antivortex at the inner edge of the nanoring, whereas the nucleated vortex core ($p = +1$) remains and travels towards the outer edge of the nanoring. Finally, in the micromagnetic simulations after $t = 30$ ns, the leading half-antivortex develops into a transverse domain wall traveling faster than the trailing half-antivortex, which is still coupled to the vortex core and dissipates energy through repeated nucleation and annihilation of a vortex core at the outer edge of the nanoring.[37]

Experimentally, we always observe the vortex domain wall configurations displayed in Figs. 2(a) and 2(b) after a clockwise or counter-clockwise rotation of the field, irrespectively of the initial configurations of the domain walls. So, similar to the case discussed above, the vortex domain wall chirality also switches if the vortex core polarity is initially $p = +1$. In this case, the gyroforce $\mathbf{G} \times \mathbf{v}$ points towards the outer edge of the ring, such that the vortex core annihilates with the leading half-antivortex and immediately renucleates with negative polarity $p = -1$. The process then continues as described above. We performed micromagnetic simulations for this case, a complete movie of the simulation can be found as supplementary movie S3.[24]

While we can qualitatively reproduce the domain wall chirality-switching by micromagnetic simulations, we only observe the effect in the simulations at higher frequencies and field amplitudes than in the experiment. One of the reasons is likely to be temperature; the simulations are all carried out at $T = 0$ K, whereas the experiments are carried out at room temperature. Because all switching events need to overcome energy barriers, it is clear that the thermal activation at room temperature helps to overcome these barriers at lower fields and frequencies than at 0 K. This explanation is further corroborated by the blurring of the magnetic contrast in the time-resolved images during the switching event, as the timing of thermally activated processes is not completely reproducible and therefore the switching process does not occur with constant timing as is required for the stroboscopic measurement technique.

We have experimentally observed that the vortex domain wall chirality above the Walker breakdown does not alternate in the ring structures,[23] and hence, the vortex chirality is fixed by the sense of rotation of the external magnetic field. Indeed, whereas the vortex core is initially displaced towards the outer edge of the ring therefore increasing the domain parallel to the radial component of the field (see Figs. 3(a) and 3(c) at 14.3 ns), the gyroforce eventually

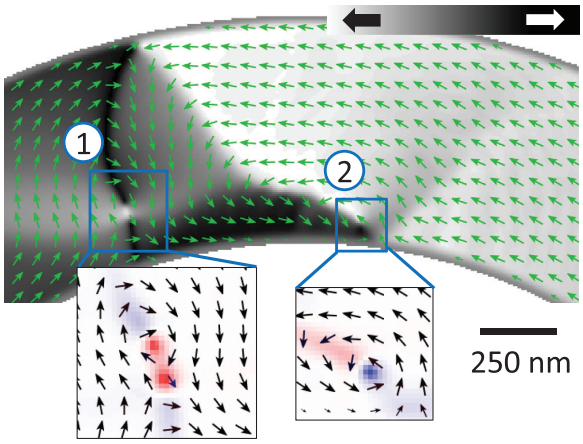

FIG. 4. Snapshot of the micromagnetic simulations during the chirality-switching process ($t = 27.5$ ns). At the leading edge of the domain wall (1), a vortex-antivortex core pair with positive polarity is nucleated. The original vortex core (2) at the trailing edge of the vortex domain wall has negative polarity. Top: The color scale indicates the magnetization component along the x-direction, black (white) indicates magnetization pointing to the right (left). Bottom (close-ups): The color scale indicates the out-of-plane magnetization component, red (blue) indicates magnetization pointing up (down).

drives the vortex core towards the inner edge of the ring, increasing the size of the domain antiparallel to the field (23.6 ns). On the other hand, once the vortex chirality and the core polarization are reversed, the leading domain wall and the radial field are aligned, stabilizing the configuration. The chirality selection is therefore determined by the radial component of the rotating field. This behavior is analogous to the chiral symmetry breaking observed in magnetic nanotubes,[38] where the domain wall propagation is enhanced or suppressed as a function of the driving field direction.

To conclude, we have observed by direct imaging that the vortex domain wall chirality can be controlled by the sense of rotation of the rotating driving field in ferromagnetic ring structures. The switching occurs in all our samples having ring widths ranging from 0.5 μm to 2 μm, ring diameters between 2 μm and 5 μm, and a thickness of 30 nm, where a vortex domain wall is formed in the onion state, and using rotating magnetic fields with frequencies between $f = 2$ MHz and 17 MHz and field strengths between $B = 4.5$ mT and 6.8 mT. We find experimentally that the switching occurs within less than 4 ns. Using micromagnetic simulations, we find that during this switching process, the original vortex core is expelled at the inner edge of the nanoring, while a vortex-antivortex core pair is nucleated at the leading 90°-Néel domain wall and only the new vortex core with opposite vortex core polarity remains. The blurring of the magnetic contrast in the time-resolved images indicates that the switching process occurs with the support of thermal activation that enables switching at room temperature for lower fields and frequencies than at 0 K. We find that the process is highly reproducible so that the domain wall chirality can be set with high fidelity in devices with curved geometries based on field-driven domain wall motion.

We thank R. Allenspach for helpful discussions. The authors acknowledge support by the German Science Foundation (DFG SFB 767, KL1811, MAINZ GSC 266), the ERC (2007-Stg 208162), the EU (MAGWIRE FP7-ICT-2009-5 257707, SpinIcur FP7-PEOPLE-2012-ITN 316657, WALL FP7-PEOPLE-2013-ITN 608031), the Center for innovative and emerging materials (CINEMA), and the Swiss National Science Foundation. Part of this work was carried out at the MAXYMUS scanning X-ray microscope at HZB, BESSY II in Berlin, Germany. The Advanced Light Source is supported by the Director, Office of Science, Office of Basic Energy Sciences, of the U.S. Department of Energy under Contract No. DE-AC02-05CH11231.

[1]S. S. P. Parkin, M. Hayashi, and L. Thomas, Science **320**, 190 (2008).
[2]D. A. Allwood, G. Xiong, C. C. Faulkner, D. Atkinson, D. Petit, and R. P. Cowburn, Science **309**, 1688 (2005).
[3]J. A. Currivan, Y. Jang, M. D. Mascaro, M. A. Baldo, and C. A. Ross, IEEE Magn. Lett. **3**, 3000104 (2012).
[4]O. Boulle, G. Malinowski, and M. Kläui, Mater. Sci. Eng. R **72**, 159 (2011).
[5]R. McMichael and M. Donahue, IEEE Trans. Magn. **33**, 4167 (1997).
[6]M. Kläui, J. Phys.: Condens. Mattter **20**, 313001 (2008).
[7]A. Wachowiak, J. Wiebe, M. Bode, O. Pietzsch, M. Morgenstern, and R. Wiesendanger, Science **298**, 577 (2002).
[8]S. Bohlens, B. Krüger, A. Drews, M. Bolte, G. Meier, and D. Pfannkuche, Appl. Phys. Lett. **93**, 142508 (2008).
[9]M. Jaafar, R. Yanes, D. Perez de Lara, O. Chubykalo-Fesenko, A. Asenjo, E. M. Gonzalez, J. V. Anguita, M. Vazquez, and J. L. Vicent, Phys. Rev. B **81**, 054439 (2010).
[10]A. Pushp, T. Phung, C. Rettner, B. P. Hughes, S.-H. Yang, L. Thomas, and S. S. P. Parkin, Nat. Phys. **9**, 505 (2013).
[11]M. Kläui, H. Ehrke, U. Rüdiger, T. Kasama, R. E. Dunin-Borkowski, D. Backes, L. J. Heyderman, C. A. F. Vaz, J. A. C. Bland, G. Faini, E. Cambril, and W. Wernsdorfer, Appl. Phys. Lett. **87**, 102509 (2005).
[12]M. Hayashi, L. Thomas, C. Rettner, R. Moriya, X. Jiang, and S. S. P. Parkin, Phys. Rev. Lett. **97**, 207205 (2006).
[13]D. Petit, A.-V. Jausovec, D. Read, and R. P. Cowburn, J. Appl. Phys. **103**, 114307 (2008).
[14]L. K. Bogart, D. Atkinson, K. O'Shea, D. McGrouther, and S. McVitie, Phys. Rev. B **79**, 054414 (2009).
[15]E.-S. Wilhelm, D. McGrouther, L. Heyne, A. Bisig, and M. Kläui, Appl. Phys. Lett. **95**, 252501 (2009).
[16]D. McGrouther, S. McVitie, J. N. Chapman, and A. Gentils, Appl. Phys. Lett. **91**, 022506 (2007).
[17]J. Rothman, M. Kläui, L. Lopez-Diaz, C. A. F. Vaz, A. Bleloch, J. A. C. Bland, Z. Cui, and R. Speaks, Phys. Rev. Lett. **86**, 1098 (2001).
[18]Y. Nakatani, A. Thiaville, and J. Miltat, J. Magn. Magn. Mater. **290–291**, 750 (2005).
[19]M. Negoita, T. J. Hayward, and D. A. Allwood, Appl. Phys. Lett. **100**, 072405 (2012).
[20]M. Curcic, H. Stoll, M. Weigand, V. Sackmann, P. Juellig, M. Kammerer, M. Noske, M. Sproll, B. Van Waeyenberge, A. Vansteenkiste, G. Woltersdorf, T. Tyliszczak, and G. Schütz, Phys. Status Solidi B **248**, 2317 (2011).
[21]A. L. D. Kilcoyne, T. Tyliszczak, W. F. Steele, S. Fakra, P. Hitchcock, K. Franck, E. Anderson, B. Harteneck, E. G. Rightor, G. E. Mitchell, A. P. Hitchcock, L. Yang, T. Warwick, and H. Ade, J. Synchrotron Radiat. **10**, 125 (2003).
[22]G. Schütz, W. Wagner, W. Wilhelm, P. Kienle, R. Zeller, R. Frahm, and G. Materlik, Phys. Rev. Lett. **58**, 737 (1987).
[23]A. Bisig, M. Stärk, M.-A. Mawass, C. Moutafis, J. Rhensius, J. Heidler, F. Büttner, M. Noske, M. Weigand, S. Eisebitt, T. Tyliszczak, B. Van Waeyenberge, H. Stoll, G. Schütz, and M. Kläui, Nat. Commun. **4**, 2328 (2013).
[24]See supplementary material at http://dx.doi.org/10.1063/1.4915256 for the series of time-resolved images and the micromagnetic simulations.
[25]A. A. Thiele, Phys. Rev. Lett. **30**, 230 (1973).
[26]D. L. Huber, Phys. Rev. B **26**, 3758 (1982).
[27]M. Laufenberg, D. Backes, W. Bührer, D. Bedau, M. Kläui, U. Rüdiger, C. A. F. Vaz, J. A. C. Bland, L. J. Heyderman, F. Nolting, S. Cherifi, A. Locatelli, R. Belkhou, S. Heun, and E. Bauer, Appl. Phys. Lett. **88**, 052507 (2006).
[28]M. Donahue and D. Porter, Interagency Report NISTIR 6376, National Institute of Standards and Technology, 1999.
[29]T. A. Moore, M. Kläui, L. Heyne, P. Möhrke, D. Backes, J. Rhensius, U. Rüdiger, L. J. Heyderman, J.-U. Thiele, G. Woltersdorf, C. H. Back, A. Fraile Rodriguez, F. Nolting, T. O. Mentes, M. A. Nino, A. Locatelli, A. Potenza, H. Marchetto, S. Cavill, and S. S. Dhesi, Phys. Rev. B **80**, 132403 (2009).
[30]R. Hertel, S. Gliga, M. Fähnle, and C. M. Schneider, Phys. Rev. Lett. **98**, 117201 (2007).
[31]A. Vansteenkiste, K. W. Chou, M. Weigand, M. Curcic, V. Sackmann, H. Stoll, T. Tyliszczak, G. Woltersdorf, C. H. Back, G. Schütz, and B. V. Waeyenberge, Nat. Phys. **5**, 332 (2009).
[32]K.-S. Lee, S.-K. Kim, Y.-S. Yu, Y.-S. Choi, K. Y. Guslienko, H. Jung, and P. Fischer, Phys. Rev. Lett. **101**, 267206 (2008).
[33]K. Y. Guslienko, K.-S. Lee, and S.-K. Kim, Phys. Rev. Lett. **100**, 027203 (2008).
[34]J. He, Z. Li, and S. Zhang, Phys. Rev. B **73**, 184408 (2006).
[35]K. Y. Guslienko, B. A. Ivanov, V. Novosad, Y. Otani, H. Shima, and K. Fukamichi, J. Appl. Phys. **91**, 8037 (2002).
[36]K. Y. Guslienko, X. F. Han, D. J. Keavney, R. Divan, and S. D. Bader, Phys. Rev. Lett. **96**, 067205 (2006).
[37]C. Zinoni, A. Vanhaverbeke, P. Eib, G. Salis, and R. Allenspach, Phys. Rev. Lett. **107**, 207204 (2011).
[38]M. Yan, C. Andreas, A. Kákay, F. García-Sánchez, and R. Hertel, Appl. Phys. Lett. **100**, 252401 (2012).